Structural Chemistry of a Green Fluorescent Protein Zn Biosensor

ARTICLE *in* JOURNAL OF THE AMERICAN CHEMICAL SOCIETY · MAY 2002

Impact Factor: 12.11 · DOI: 10.1021/ja0176954 · Source: PubMed

4 AUTHORS, INCLUDING:

David P Barondeau
Texas A&M University
29 PUBLICATIONS **1,134** CITATIONS
SEE PROFILE

John Tainer
University of Texas MD Anderson Cancer Center
458 PUBLICATIONS **30,197** CITATIONS
SEE PROFILE

J|A|C|S
COMMUNICATIONS

Published on Web 03/15/2002

Structural Chemistry of a Green Fluorescent Protein Zn Biosensor

David P. Barondeau, Carey J. Kassmann, John A. Tainer, and Elizabeth D. Getzoff*

Department of Molecular Biology, The Skaggs Institute for Chemical Biology, The Scripps Research Institute, 10550 North Torrey Pines Rd., La Jolla, California 92037

Received December 6, 2001

Zinc metalloproteins influence DNA synthesis, microtubule polymerization, gene expression, apoptosis, and immune system function.[1] Furthermore, Zn(II) homeostasis is critical for complex neurobiological systems: Zn(II) acts in synaptic transmission, as a contributory factor in neurological disorders including epilepsy and Alzheimer's disease, and as a neurotoxin under seizure or pathological conditions.[1] To fully understand Zn(II) functions in cell and neurobiology, probes are needed that are capable of monitoring in vivo spatial and temporal distributions of metal ions. Designed small molecule Zn(II) fluorescent probes have many advantages.[2] However, protein-based biosensors[3] might complement these probes as proteins can be optimized for selectivity and affinity, added noninvasively to cells by transfection, and targeted to specific tissues, organelles, or cellular locations. Recently, proteins have been engineered to incorporate desired properties via structure-based[4] and directed evolution[5] strategies. Since protein metal site specificity and activity are exquisitely sensitive to precise ligand chemistry and geometry, structure-based design of metal ion biosensors would benefit from very high resolution structures of apo and distinct metal-bound protein states. We report here (i) the design and characterization of a green fluorescent protein (GFP) mutant that binds Zn(II) (enhancing fluorescence intensity) and Cu(II) (quenching fluorescence) to a tridentate chromophore resembling half a porphyrin and (ii) very high-resolution crystallographic structures for these apo, Zn(II)-bound, and Cu(II)-bound proteins (Figure 1). These structures, reported with experimentally determined standard uncertainty errors, define accurate metal-site geometric parameters for a novel GFP metal-binding site and provide critical structural chemistry for understanding the metal ion affinity, specificity, and activity of protein metal sites. Moreover, these results prompt structure-based hypotheses to explain the protein's metal ion selectivity, metal binding kinetics, and fluorescence enhancement upon Zn(II) binding, with potential general implications for the design of protein metal ion biosensors.

The GFP fluorophore is self-synthesized within the center of an antiparallel β-barrel from protein residues Ser65, Tyr66, and Gly67.[6,7] The chromophore has a high fluorescence quantum yield (0.79) and an emission maximum at 508 nm.[6] Mutated proteins, such as Y66H Y145F, can still generate a chromophore, but with modified emission wavelengths (447 nm) and quantum yields (0.38).[8] The self-generated fluorophore makes GFP an ideal system for screening directed libraries of random mutants for desirable characteristics such as increased soluble expression or altered spectral properties.[6] Thus, the engineering of a specific metal binding site in GFP that couples metal binding to modified fluorescent signals provides a prototype suitable for optimization of kinetic and thermodynamic properties by directed evolution strategies. To create this prototype, we combined porphyrin-like metal ligand, protein solubility, and accessibility design criteria with high-resolution structure determination and analysis.

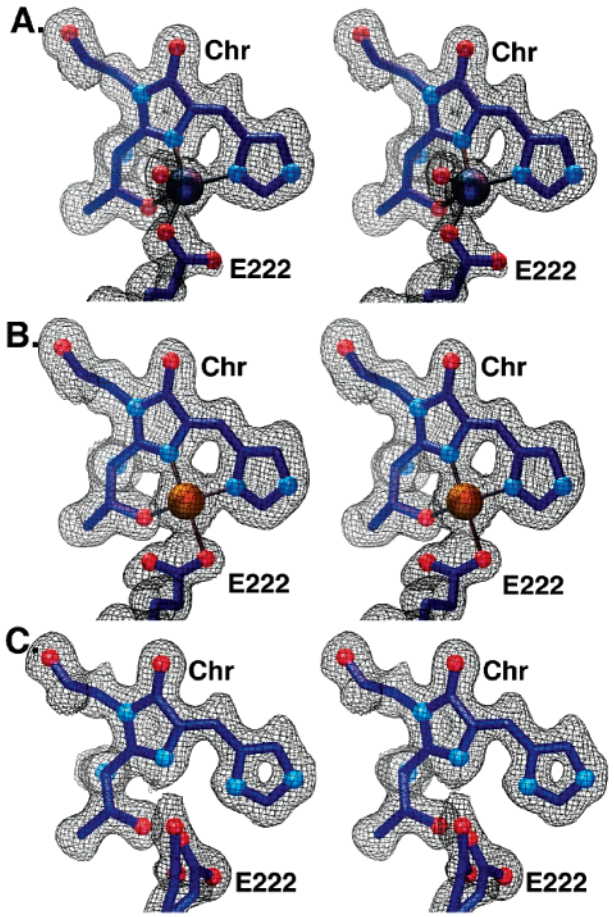

Figure 1. Stereopairs of BFPms1 metal binding sites and 2Fo−Fc electron density maps contoured at 1 σ for (A) Zn-bound (1.44 Å), (B) Cu-bound (1.50 Å), and (C) apo (1.35 Å) structures. Images made with AVS.

To link metal ion binding to chromophore spectroscopic properties, our first structure-based metal site design (BFPms1) includes the BFP chromophore (Y66H), which resembles a dipyrrole unit of porphyrin.[9a] In addition, mutations were included for higher quantum yield (Y145F),[8] increased solubility (F64L, F99S, M153T, and V163A),[6] faster chromophore formation (S65T),[6] and creating a hole into the β-barrel (H148G)[9b] to improve metal binding kinetics. The metal site appears specific for Cu (24 μM K_D) and Zn (50 μM K_D), as no other divalent first row transition metal binds at metal concentrations up to 2 mM. Moreover, Zn(II) and Cu(II) each alter chromophore spectroscopic properties in distinct ways. Zn(II) binding increases fluorescence intensity 2-fold, but does not alter the absorbance spectra. In contrast, Cu(II) binding quenches

* Address correspondence to this author. E-mail: edg@scripps.edu.

10.1021/ja0176954 CCC: $22.00

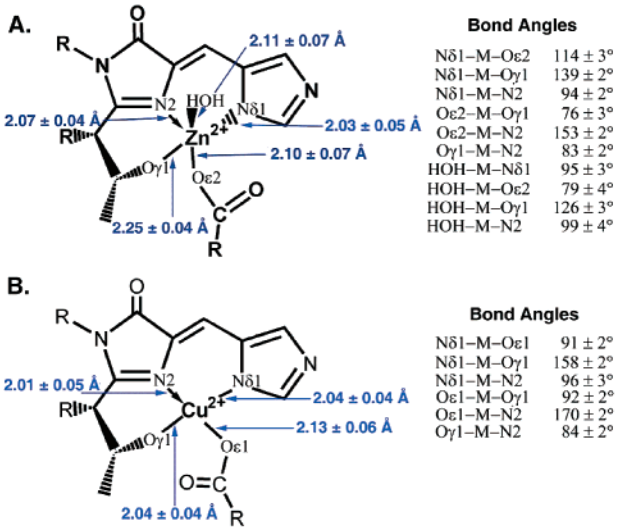

Figure 2. BFPms1 coordination geometry with experimentally defined standard uncertainty errors for (A) Zn-bound and (B) Cu-bound structures. Bond lengths are displayed in blue. Images rendered with ChemDraw (CambridgeSoft Corporation).

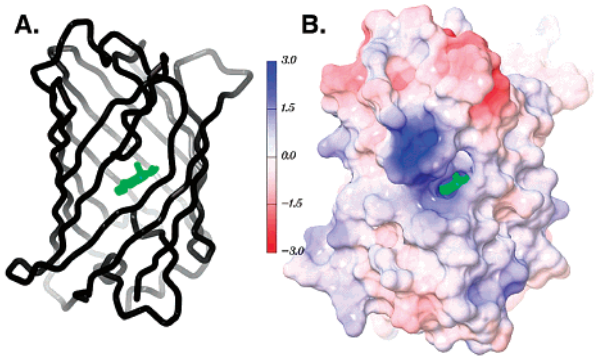

Figure 3. BFPms1 overall structure, channel, and electrostatic surface: (A) overall fold displaying the Cα trace (black) and the chromophore (green) and (B) electrostatic potential displayed in red (negative) and blue (positive) mapped onto the protein molecular surface. The chromophore is shown in green. Units are in kcal mol^{-1} e^{-1}. Parts A and B are in the same orientation and made with AVS.

fluorescence and shifts the absorbance maximum from 379 to 444 nm. Thus, BFPms1 provides the basic features for an effective Zn(II) biosensor: good photophysical properties, an increase in signal upon analyte binding, and reasonable specificity. Further optimization may allow BFPms1 to detect in vivo Zn(II) concentrations, which range from subnanomolar within the cytoplasm to millimolar in some vesicles, and high micromolar concentrations in gray matter and nerve synapses.[1]

To understand the structural basis for metal-induced spectroscopic changes and metal ion selectivity, we determined very high-resolution apo and metal-bound crystallographic structures that provide unusually accurate protein metal site geometries. Most metalloprotein structures are at resolutions worse than 1.5 Å, requiring restrained refinements that potentially bias metal site geometric parameters. The resolution of our structures allowed us to refine metal centers without geometric restraints, determine experimentally defined standard uncertainty errors for bond lengths and angles (Figure 2), and anisotropically model thermal displacement parameters (*B*-values).

The 1.44 Å resolution structure of Zn-bound BFPms1 (PDB code 1KYS) reveals a 5-coordinate Zn(II) site with distorted trigonal bipyramidal geometry (Figures 1A, 2A). The metal ion binds tridentate to the chromophore (Chr), to the side-chain of Glu222, and to a water molecule. The trigonal plane formed by chromophore atoms Nδ1 and Oγ1 and the water molecule is perpendicular to the plane of the chromophore. The H_2O−Zn−Nδ1 angle of 95 ± 3° shows the largest deviation from perfect trigonal bipyramidal geometry (120°). The metal ligand bond lengths resemble those in other metalloprotein structures in the Metalloprotein Database and Browser (MDB)[10] (Zn−N, 2.11 ± 0.15 Å, n = 3516; Zn−O 2.13 ± 0.19 Å, n = 2734) except for the longer Zn−Oγ1 bond (2.25 ± 0.04 Å), which might reflect geometric constraints, but more probably reflects protonation of Oγ1. Searching Zn−O(H)-CR in the high-resolution, small-molecule Cambridge Structural Database (CSD) revealed that, consistent with the BFPms1 Zn−Oγ1 bond, protonated oxygens exhibit longer (weaker) Zn−oxygen bonds (2.16 ± 0.11 Å, n = 82) than do deprotonated oxygens (2.08 ± 0.14 Å, n = 1087). Furthermore, the hydrogen-bonding distance from Chr Oγ1 (derived from Thr65 hydroxyl) to a main-chain carbonyl oxygen is unchanged from apo to Zn-bound BFPms1 (3.08 Å). Although a Chr Cα−Cβ bond rotation of Oγ1 would accommodate a shorter (stronger) Zn−Oγ1 bond to a deprotonated oxygen ligand, the Chr Oγ1 hydrogen bond would be lost. The structure suggests that a protonated Zn−Oγ1 ligand with a hydrogen bond is favored over a deprotonated ligand without one.

In the 1.50 Å resolution structure of Cu(II)-bound BFPms1 (PDB code 1KYR), Cu(II) has square-planar geometry (Figures 1B and 2B), similar to metalated porphyrins, and exhibits a Jahn−Teller distortion moving the axial water molecule out of the primary coordination sphere. The Cu(II) ligand geometry does not deviate far from square planar, with the Oγ1−Cu−N2 (84 ± 2°) and Nδ1−Cu−N2 (96 ± 3°) angles showing the largest distortions from 90°. The metal ligand distances are similar to those in the MDB (Cu−O, 2.16 ± 0.20 Å, n = 291; Cu−N, 2.08 ± 0.12 Å, n = 1489). In contrast to Zn−Oγ1, the Cu−Oγ1 bond length (2.04 ± 0.04 Å) is more consistent with CSD Cu−O(H)CR deprotonated (2.02 ± 0.18 Å, n = 4762) than protonated (2.22 ± 0.21 Å, n = 339) distances. Further, the distance from the Chr Oγ1 atom to the backbone carbonyl (3.14 Å) is longer than in the apo and Zn-bound structures. The data suggest a deprotonated Cu−Oγ1 ligand. Metalloproteins with threonine side chain ligation are rare, with one Zn(II) (alkaline phosphatase) and no copper examples in the MDB, underscoring the novel aspects of this GFP metal site.

The 1.35 Å resolution structure of apo BFPms1 (PDB code 1KYP) reveals the designed channel, made by mutation H148G, extending through the β-barrel to the buried chromophore (Figure 3). Despite this open channel, metal insertion rates are remarkably slow ($t_{1/2}$ > 4 h), likely due to electrostatic repulsion of the metal cation by a large positive region near the channel entrance (Figure 3B). Analogously, the superoxide dismutase turnover rate can be increased when negative charge is removed from the superoxide anion substrate channel.[11a] Electrostatics at the metal center can also influence metal binding kinetics. In carbonic anhydrase, mutation of a second shell residue stabilizes a metal-ligating histidine as an anion and increases the metal insertion rate.[11b] In fact, metal ion transfer, insertion, and occupancy in vivo are proposed to be under kinetic rather than thermodynamic control, based on extremely tight binding of bacterial Zn(II) homeostasis regulatory proteins.[12] Directed evolution of proteins such as BFPms1, whose metal-binding properties are linked to a fluorescent signal, allows identification of variants with different metal insertion rates, which may help determine controlling factors for metal-binding kinetics.

The observed metal ion selectivity of the BFPms1 site probably reflects a combination of thermodynamic factors, including coordination chemistry and metal−ligand pK_a properties, plus kinetic

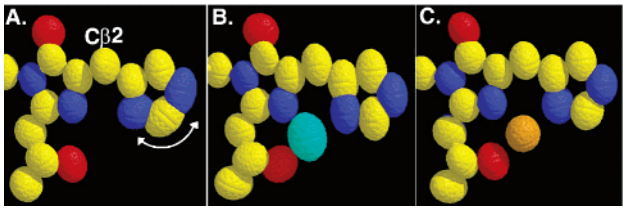

Figure 4. Anisotropic thermal displacement parameters of the BFPms1 chromophore validate metal-induced rigidification leading to fluorescence changes. Thermal ellipsoids representing individual *B*-factors displayed for (A) apo (40% probability), (B) Zn-bound (26.7% probability), and (C) Cu-bound (22.5% probability) BFPms1.

barriers inherent in transition metal binding to porphyrin-like ligands. The BFPms1 metal site selectivity follows the Irving−Williams series,[13a] Zn < Cu > Ni > Co > Fe, in that Cu > Zn and the other metal ions do not appear to bind. Yet, in porphyrin chemistry, the divalent metal ion stability order for a square-planar geometry favors the d^8 configuration of Ni(II), Ni > Cu > Co > Fe > Zn.[13b] Therefore, we further tested the selectivity against Ni(II) by soaking BFPms1 crystals in 50 mM $NiCl_2$, but observed no metal binding to the chromophore. The apparent lower pK_a for the Chr Oγ1 atom in Cu(II) vs Zn(II) BFPms1 is consistent with the relative pK_a values for divalent hexa-aquo Cu (7.5), Ni (9.4), Zn (9.6), Co (9.6), and Fe (10.1) complexes.[13c] This suggests that Ni(II), Co(II), and Fe(II), like Zn(II), would bind to BFPms1 with a protonated Chr Oγ1 ligand. However, Zn(II), unlike Ni(II), Co(II), or Fe(II), has a d^{10} configuration and no ligand field stabilization energy, which allows the metal to bind with distorted trigonal bipyramidal geometry. Finally, since our metal binding kinetics are slow, if metal insertion rates follow the metalloporphyrin trend, Cu(II) > Co(II) > Fe(II) > Ni(II),[13d] kinetic barriers may also contribute to the observed selectivity.

The apo and metal-bound BFPms1 crystallographic structures resolve the apparent paradox that the chromophore ligand is preorganized for both Zn and Cu binding, yet these metal ions bind with very different coordination geometries. The primary structural differences in metal site geometry come from the metal ion, rather than from the protein ligands. The Zn(II) is positioned 0.4 Å farther from the plane of the chromophore, and closer to its additional water ligand. The protein adjusts to Zn(II) and Cu(II) binding primarily by distinct rearrangements of E222, which has multiple conformations in the apo structure (Figure 1C). Also, a subtle (12°) rotation of the Chr imidazole ring better aligns the Chr Nδ1 atom for Cu(II) binding. Importantly, for metal ion biosensor design, our structures suggest that both Zn and Cu metal site geometries rigidify the BFPms1 chromophore (Figure 4), resulting in increased fluorescence intensity upon Zn binding.

The high-resolution structures of apo, Zn-bound, and Cu-bound BFPms1 provide an experimental validation of the metal ion mediated modulation of chromophore flexibility. The anisotropic *B*-values for BFPms1 apo and metal-bound structures show that the chromophore imidazole displays significantly less rotational motion when metal ion is bound (Figure 4). Comparison of the *B*-values at different probability levels, based on scaling by Wilson *B*-factors, accounted for differences in lattice disorder between crystals (details in the Supporting Information). In the apo structure, the Chr (His66) imidazole lacks protein hydrogen bond partners, probably due to its smaller size than wild-type Tyr66, and pivots about the Cβ2 atom (Figure 4A). In the metal-bound structures (Figure 4B,C), the decreased chromophore mobility limits dissipation of excited-state energy through thermal relaxation pathways. In addition, the chromophore in the apo structure is less planar (0.10 Å average deviation from a least-squares plane) than in the Zn-bound (0.08 Å) or Cu-bound (0.07 Å) structures. On the basis of these results, metal binding rigidifies the chromophore imidazole, locking it into a discrete and more planar conformation, thereby increasing the fluorescence quantum yield upon Zn(II) binding. Cu(II) binding also rigidifies the chromophore, but since it is d^9, it quenches fluorescence likely through an electron-transfer mechanism.

In sum, we have designed and characterized the structural chemistry of a protein metal ion biosensor (BFPms1) that (i) incorporates a novel porphyrin-like fluorophore as a tridentate ligand and (ii) preferentially binds Zn(II) and Cu(II) with different coordination geometries and distinguishable spectroscopic properties. Moreover, our high-resolution apo, Zn(II)-bound, and Cu(II)-bound protein structures reveal how structure-based design has effectively linked metal binding to changes in fluorescence properties. Thus this protein Zn(II) biosensor provides a prototype suitable for further optimization by directed evolution to generate metalloproteins with desirable physical or biochemical properties for significant scientific and medical applications.

Acknowledgment. We thank the La Jolla Interfaces in Science and NIH GM19290 Postdoctoral Fellowships (D.P.B.), NIH grant GM48495, and the Stanford Synchrotron Radiation Laboratory for support. We thank S. Falkow for GFP constructs and C. D. Putnam, V. A. Roberts, C. A. Mullen, J. M. Castagnetto, T. I. Wood, J. L. Tubbs, and M. G. Finn for scientific discussions.

Supporting Information Available: Preparation of BFPms1, determination of the binding constants and kinetics, crystallographic data collection and refinement statistics, details of the electrostatic potential and anisotropic *B*-value calculations, and general method references (PDF). This material is available free of charge via the Internet at http://pubs.acs.org.

References

(1) (a) Cuajungco, M. P.; Lees, G. J. *Neurobiol. Dis.* **1997**, *4*, 137−69. (b) Vogt, K.; Mellor, J.; Tong, G.; Nicoll, R. *Neuron* **2000**, *26*, 187−96.
(2) Burdette, S. C.; Lippard, S. J. *Coor. Chem. Rev.* **2001**, 216−7, 333−61.
(3) (a) Baird, G. S.; Zacharias, D. A.; Tsien, R. Y. *Proc. Natl. Acad. Sci.* **1999**, *96*, 11241−6. (b) Nair, S. K.; Elbaum, D.; Christianson, D. W. *J. Biol. Chem.* **1996**, *271*, 1003−7.
(4) (a) Lu, Y.; Berry, S. M.; Pfister, T. D. *Chem. Rev.* **2001**, *101*, 3047−80. (b) Benson, D. E.; Conrad, D. W.; de Lorimer, R. M.; Trammell, S. A.; Hellinga, H. W. *Science* **2001**, *293*, 1641−4. (c) Farinas, E.; Regan, L. *Protein Sci.* **1998**, *7*, 1939−46. (d) Lombardi, A.; Summa, C. M.; Geremia, S.; Randaccio, L.; Pavone, V.; DeGrado, W. F. *Proc. Natl. Acad. Sci.* **2000**, *97*, 6298−305.
(5) Joo, H.; Lin, Z.; Arnold, F. H. *Nature* **1999**, *399*, 670−3.
(6) Tsien, R. Y. *Annu. Rev. Biochem.* **1998**, *67*, 509−44.
(7) Ormo, M.; Cubitt, A. B.; Kallio, K.; Gross, L. A.; Tsien, R. Y.; Remington, S. J. *Science* **1996**, *273*, 1392−5.
(8) Heim, R.; Tsien, R. Y. *Curr. Biol.* **1996**, *6*, 178−82.
(9) (a) Wachter, R. M.; King, B. A.; Heim, R.; Kallio, K.; Tsien, R. Y.; Boxer, S. G.; Remington, S. J. *Biochemistry* **1997**, *36*, 9759−65. (b) Wachter, R. M.; Elsliger, M.; Kallio, K.; Hanson, G. T.; Remington, S. J. *Structure.* **1998**, *6*, 1267−77.
(10) MDB Metalloprotein Database and Browser (http://metallo.scripps.edu): Castagnetto, J. M.; Hennessy, S. W.; Roberts, V. A.; Getzoff, E. D.; Tainer, J. A.; Pique, M. E. *Nucleic Acids Res.* **2002**, *30*, 379−82.
(11) (a) Getzoff, E. D.; Cabelli, D. E.; Fisher, C. L.; Parge, H. E.; Viezzoli, M. S.; Banci, L.; Hallewell, R. A. *Nature* **1992**, *358*, 347−51. (b) Huang, C.; Lesburg, C. A.; Kiefer, L. L.; Fierke, C. A.; Christianson, D. W. *Biochemistry* **1996**, *35*, 3439−46.
(12) (a) Hitomi, Y.; Outten; C. E.; O'Halloran, T. V. *J. Am. Chem. Soc.* **2001**, *123*, 8614−5. (b) VanZile, M. L.; Cosper, N. J.; Scott, R. A.; Giedroc, D. P. *Biochemistry* **2000**, *39*, 11818−29.
(13) (a) Irving, H.; Williams, R. J. P. *Nature* **1948**, *162*, 746−7. (b) Sigel, H.; McCormick, D. B. *Acc. Chem. Res.* **1970**, *3*, 201−8. (c) Yatsimirksii, K. B.; Vasil'ev, V. P. *Instability Constants of Complex Compounds*; Pergamon: Elmsford, NY, 1960. (d) Kingham, D. J.; Brisbin, D. A. *Inorg. Chem.* **1970**, *9*, 2034−7.

JA0176954